Advanced Composites and Hybrid Materials
https://doi.org/10.1007/s42114-022-00447-w

ORIGINAL RESEARCH

Tunable multichannel terahertz perfect graphene absorber with Fibonacci quasiperiodic photonic crystal

Jun Wu[1,2] · Xiuwei Yang[3] · Zhongmin Wang[3] · Biyuan Wu[4,5] · Xiaohu Wu[5]

Received: 27 December 2021 / Revised: 8 February 2022 / Accepted: 2 March 2022

Abstract
Tunable multichannel perfect absorption in monolayer graphene at terahertz frequencies is studied, which is realized through depositing a graphene monolayer on a Fibonacci quasiperiodic multilayer structure separated by a spacer. Three absorption peaks with absorptivity larger than 95% are obtained, which is attributed to the graphene Tamm plasmon polaritons and multiple photonic stopbands of dielectric Fibonacci multilayers. And the distributions of the electric field intensity are investigated to reveal the physical origin. Besides, the multichannel operating frequencies can be flexibly tuned through varying the angle of incidence and structure dimensions of the absorber, and it is found the absorption is not sensitive to the polarization state. In addition, the multichannel perfect absorption could be tuned to different frequencies through merely a change in the Fermi energy and the absorption performance could be flexibly extended to various channels of different number without re-optimizing the structure dimensions. We believe that the conclusions may find significant applications for the realization of novel tunable optoelectronic devices.

Keywords Graphene · Tamm plasmon polaritons · Fibonacci multilayers · Spectrum selective absorption

1 Introduction

Terahertz (THz) wave usually refers to the frequency within 0.1–10 THz, which shares similarities with both the far infrared and microwave frequencies. It has attracted great research interests recently, thanks to its important applications in many areas, such as spectroscopy, communication, sensors, and imaging [1–3]. Among these developed devices, THz absorbers have been extensively studied recently for imaging, detecting, and sensing purposes [4–7]. The perfect absorption of THz wave is crucial for the realization of THz properties. Therefore, over the past few years, much effort has been made to achieve near-complete absorption in THz ranges by employing various geometries and materials, including hyperbolic material [8], photonic-crystal slab [9], metamaterial [10], and metasurface [11]. Though there are a large number of studies into developing THz absorber, it is highly desirable to explore novel structure combined with new materials to achieve more advanced absorption properties.

Graphene, a two-dimension material with a monolayer carbon atom, has attracted wide attentions in recent years as a potential material for developing tunable THz devices owing to its exceptional electrical, mechanical, and optical properties [12–19]. In the THz regions, the most remarkable property of graphene is that its surface conductivity could be continuously changed in a wide frequency range in virtue of chemical or electrostatic gratings. Such properties make it a promising candidate for developing tunable devices [20–22]. In addition, strong surface plasmon polaritons (SPPs) could be excited in graphene with appropriate doping, which results in tight field confinement nearby [23]. To exploit these properties for device applications, such as

✉ Jun Wu
mailswj2011@163.com

✉ Xiaohu Wu
xiaohu.wu@iat.cn

1 College of Electrical Engineering, Anhui Polytechnic University, Wuhu 241000, China

2 Department of Physics, Zhejiang University of Science and Technology, Hangzhou 310023, China

3 Institute of Automation, Qilu University of Technology (Shandong Academy of Sciences), Jinan 250014, China

4 School of Automation and Information Engineering, Xi'an University of Technology, Xi'an 710048, Shaanxi, China

5 Shandong Institute of Advanced Technology, Jinan 250100, China

Published online: 11 March 2022

perfect absorbers [24, 25], modulators [26], sensors [27], photodetectors [28], and plasmonically induced transparency [29], significant recent efforts have focused on enhancing light absorption in monolayer graphene due to the extremely weak interaction between the graphene and the incoming wave. For this purpose, many novel methods have been proposed to realize tunable THz perfect absorption. Zhang et al. designed a tunable THz absorber consisting of the combination of metallic metamaterial with double layer graphene wires, which realizes near-complete absorption with spectral tuning at THz frequency [30]. Deng et al. demonstrated that the THz absorption based on graphene heterostructure could be tuned continuously from 0 to 100% [31]. He et al. designed a THz absorber in the form of patterned graphene-SiO_2-Si-dielectric-metal structure and founded that near perfect absorption could be obtained through choosing suitable geometric dimensions and the Fermi energy of graphene [32]. Zhu et al. proposed a general mechanism, where angle-selective near-complete absorption in graphene can be achieved [33]. However, these absorbers mentioned above are typically operated with merely one absorption channel [30–33], which hinders their promising applications in various fields, such as multi-spectra channel detecting, multiparameter sensors, as well as dense wavelength-division multiplexing communication where multi-channel with narrow bandwidth is required. Gao et al. designed a multichannel absorber in the form of a spacer sandwiched between a structured graphene and a ground plane [34]. But the quality factor is small. Wang et al. reported an efficient mechanism to achieve multichannel tunable near-complete THz absorption with a graphene-1D photonic crystal structure [35]. However, only 1D period structure is considered.

Here, a tri-band tunable THz perfect graphene absorber, in the form of a monolayer graphene separated from a 1D Fibonacci quasiperiodic photonic crystal by a spacer, is proposed and studied. We show that the absorption in graphene monolayer can reach above 95% at three different frequencies. To confirm the physical origin, the distributions of electric field intensity at the three peak frequencies are illustrated. Moreover, the influences of the angle of incidence and the structure dimensions on the absorption performance are also studied so as to present the flexible tunability of the designed absorber. Finally, it is shown that the multichannel near-complete absorption not only could be dynamically tuned in virtue of the external gate voltages but also can be extended to various absorption channels by adjusting the Fibonacci order.

2 Design and results

The proposed tunable absorber is composed of a graphene monolayer, a dielectric spacer (C), and a Fibonacci quasiperiodic photonic crystal backed with a substrate, as shown in Fig. 1. The Fibonacci quasiperiodic photonic crystal consists of two dielectric layers A and B arranged according to the following rule [36]:

$$\begin{aligned} F_1(n) &= S_1 = B \\ F_2(n) &= S_2 = B^{n-1}A \\ F_3(n) &= S_3 = \left(B^{n-1}A\right)^n B \\ F_j(n) &= S_j = S_{j-1}{}^n A_{j-2} \end{aligned} \tag{1}$$

where j is the generation number and n denotes the Fibonacci order. Both of which are positive integers. The refractive indexes of A and B are $n_a = 1.45$ (SiO_2) and $n_b = 3.48$ (Si), respectively. And their thicknesses denote as h_a and h_b, respectively. The refractive indexes of C and the substrate are both equal to 1.45 (SiO_2). h_1 is the distance between graphene and 1D Fibonacci quasiperiodic photonic crystal. A TE-polarized and a TM-polarized (with the electric field and the magnetic field paralleled to the y-axis, respectively) THz waves are incoming from the air with an angle θ. Here, θ is

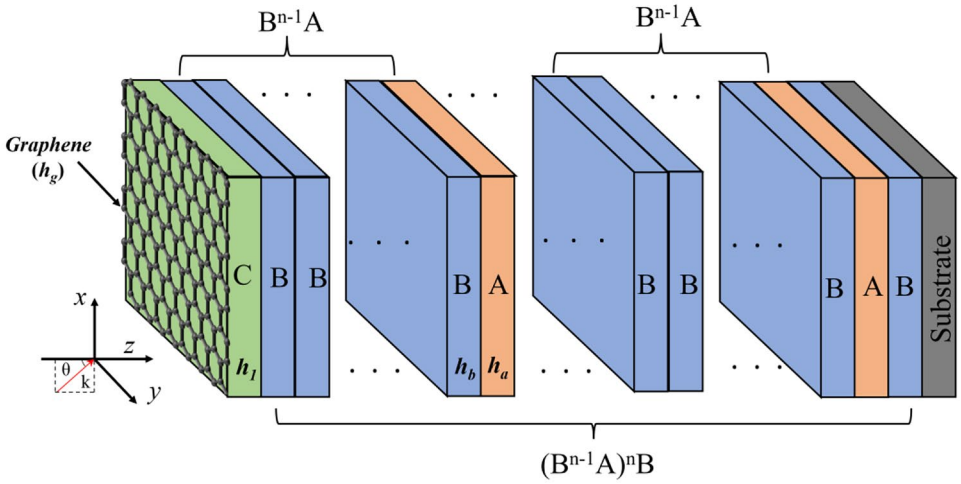

Fig. 1 Schematic of the designed graphene absorber. C is the spacer between graphene and the 1D Fibonacci multilayer

the angle between the incident wave vector and the normal direction of the structure. The incident plane is x–z plane.

The graphene layers present a frequency-dependent conductivity:

$$\sigma(\omega) = \sigma_{\text{inter}}(\omega) + \sigma_{\text{intra}}(\omega), \tag{2}$$

where $\sigma_{intra}(\omega)$ denotes the intraband contribution, and $\sigma_{inter}(\omega)$ denotes the interband contribution. For the THz frequency considered in this work and at room temperature, the interband transitions can be neglected. Thus, the surface conductivity of graphene could be approximated as [37, 38]:

$$\sigma(\omega) = \frac{e^2 E_f}{\pi\hbar^2}\frac{i}{\omega + i\tau^{-1}}, \tag{3}$$

where E_f denotes the Fermi energy, $\hbar$ denotes the reduced Planck's constant, and k_B is the Boltzmann's constant, τ denotes the carrier relaxation lifetime, e denotes the basic electric charge, and ω denotes the angular frequency. In this work, τ is chosen as 0.8 ps, and the initial Fermi energy E_f is chosen as 0.85 eV.

During the simulation, the monolayer graphene is taken as an ultra-thin layer with $h_g = 0.34$ nm and has an equivalent permittivity:

$$\varepsilon_g = 1 + \frac{i\sigma(\omega)}{\varepsilon_0 \omega h_g}, \tag{4}$$

here ε_0 denotes the vacuum dielectric constant.

The rigorous coupled-wave analysis (RCWA) is employed to design and optimize the tunable multichannel graphene THz absorber [39, 40]. In this work, j is selected as 3, as shown in Fig. 1. To construct a tri-band graphene absorber, n is set as 6. The optimized parameters of the unit cell with operating frequencies at about $f_1 = 0.9045$ THz, $f_2 = 1.0855$ THz, and $f_3 = 1.26$ THz are listed as follows: $h_1 = 86$ μm, $h_a = 46$ μm, and $h_b = 36$ μm. The simulated absorption spectra $A(f)$ can be obtained from the reflection spectra $R(f)$ and transmission spectra $T(f)$ by $A(f) = 1 - R(f) - T(f)$. Figure 2 illustrates the calculated absorption spectra for normally incident TE-polarized and TM-polarized waves. Here, the absorption spectra for both normally incident polarized waves are identical due to the symmetry of the structure. It is found that three-channel near-complete absorption is achieved with resonant frequencies at $f_1 = 0.9045$ THz, $f_2 = 1.0855$ THz, and $f_3 = 1.26$ THz and their corresponding absorbance of 94.9%, 99.94%, and 95.52%. The bandwidths are approximate 0.0085 THz, 0.022 THz, and 0.011 THz, and the quality factors ($Q = f/\Delta f$) are 106.4, 49.3, and 114.5, respectively, which all exhibit narrow frequency bandwidth.

To reveal the physical mechanism, in Fig. 3, we show the distributions of electric field intensity at three peak frequencies. In Fig. 3a, we illustrate the distributions of

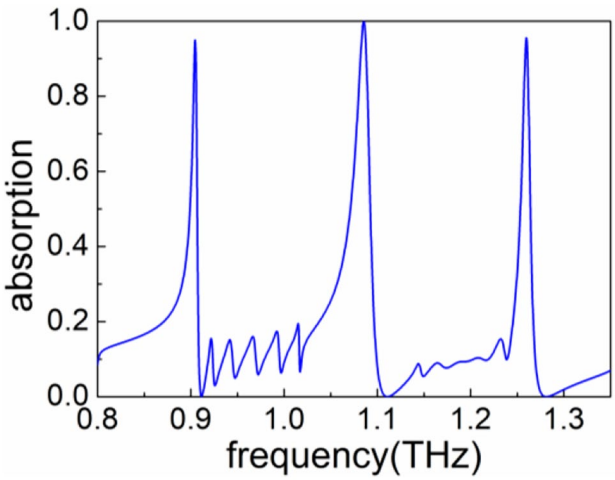

Fig. 2 Simulated absorption spectra of the proposed tunable absorber for normally incident light

normalized electric field intensity along the z-axis at frequency f_2 for the absorber without the covering of graphene. As illustrated in Fig. 3a, the electric field in the air shows an obvious profile of standing wave, which results from the superimposition of the incoming wave and the reflection wave. This indicates that near-complete reflection appears at the interface between air and the Fibonacci multilayers. However, the electric field decays gradually in the Fibonacci multilayers and the electric field enhancement at the boundary between the air and Fibonacci multilayers is extremely weak, as the Tamm plasmon polaritons (TPPs) cannot be excited at present. TPPs are a relatively new category of surface wave excited at the interface between two objects with high reflection [41, 42]. In contrast to typical SPPs, TPPs could be excited for both TE-polarized and TM-polarized waves without the assistance of external photonic structures [43]. From Fig. 3b–d, it is found that the electric fields at the resonant frequencies are strongly enhanced and mainly confined in the spacer between graphene and Fibonacci multilayers when a graphene monolayer is deposited on the Fibonacci multilayers, which is attributed to the excitation of graphene TPPs. Thus, as the sole dissipative material in the structure, graphene could strongly absorb the incoming THz wave, which is also confirmed by the intensity profile where hardly any electric field of the reflecting wave is found in the air. The perfect multichannel absorption in the monolayer graphene can be attributed to the graphene TPPs.

3 Discussion

Next, we study the effect of the angle of incidence on the light absorption in graphene. The simulated absorption spectra for $\theta = 0°$, 20°, and 40° for TE polarization

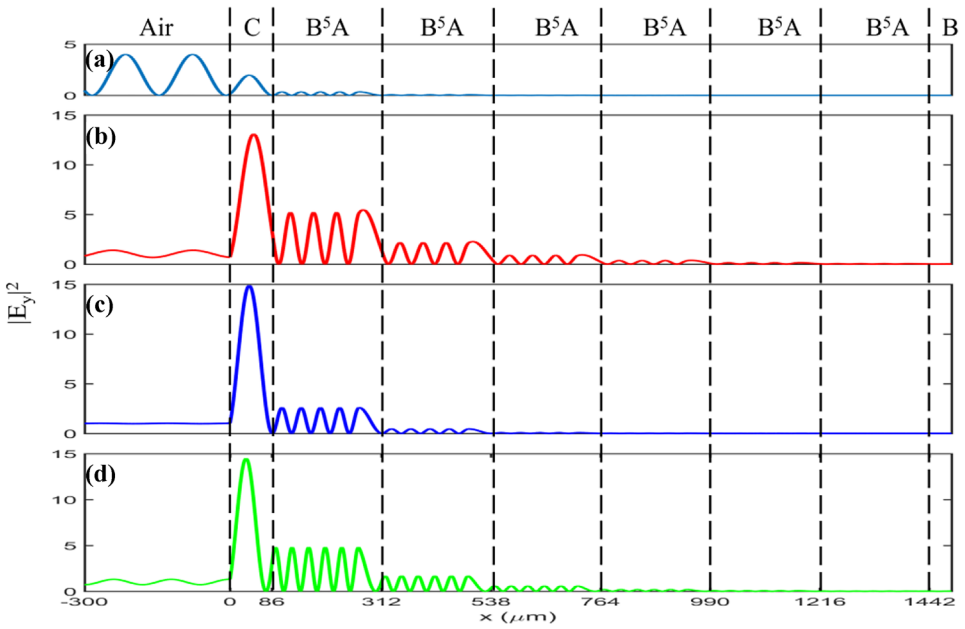

Fig. 3 The distributions of normalized electric field intensity: (**a**) f_2; (**b**) f_1; (**c**) f_2; (**d**) f_3. There is no graphene in (**a**), while there is graphene in (**b**)–(**d**)

and TM polarization are shown in Fig. 4a and b, respectively. Clearly, three resonant peaks for both polarizations exhibit a blueshift with the increase of the incident angle, as the photonic stopbands of Fibonacci multilayers move to larger frequency with the incident angle increase [44]. Though with a little decrease or increase for different absorption peaks, the incident angle can be considered as an efficient method to tune the operating frequencies of the designed graphene absorber. It should be noted that the three-channel absorption for both polarizations remain stable with the angle of incidence changing from 0 to 40°, indicating that perfect multichannel absorptions are not sensitive to the polarization state of the incoming light. Such advantage is beneficial for real applications.

Furthermore, to guide the actual manufacturing, we depict the effects of structure dimensions on the absorption performance. In Fig. 5, we show the calculated absorption spectra versus the change of h_a, h_b, n_a, and n_b, respectively. All of three resonant peaks show a redshift when increasing h_a or h_b, as illustrated in Fig. 5a and b. Though with a little decrease or increase for different absorption peaks, the absorptions remain above 90% in the considered parameter ranges. As presented in Fig. 5c and d, all of the three resonant peaks move to the smaller frequencies when increasing n_a or n_b. Clearly, the redshift caused by increasing $h_b(n_b)$ is much larger than that by increasing $h_a(n_a)$. Such phenomenon stems from that the shift of photonic stopband with the increasing of $h_b(n_b)$ is larger than that by increasing $h_a(n_a)$, which has been explained by a technology based on the Fourier transform of the structure index profile [36]. Figure 6 presents the absorption performance with the change of h_1. We can see that the absorption exhibits a redshift when h_1 increases from 84 to 88 μm, though with a little decrease or increase for different absorption peaks. In general, the perfect multichannel absorption properties remain excellent within

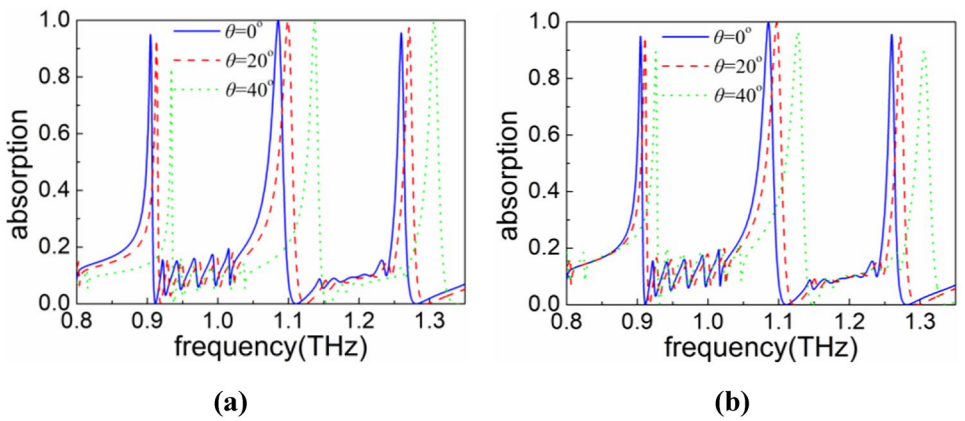

Fig. 4 The simulated absorption spectra for (**a**) TE-polarized wave and (**b**) TM-polarized wave at θ = 0°, 20°, and 40°, respectively

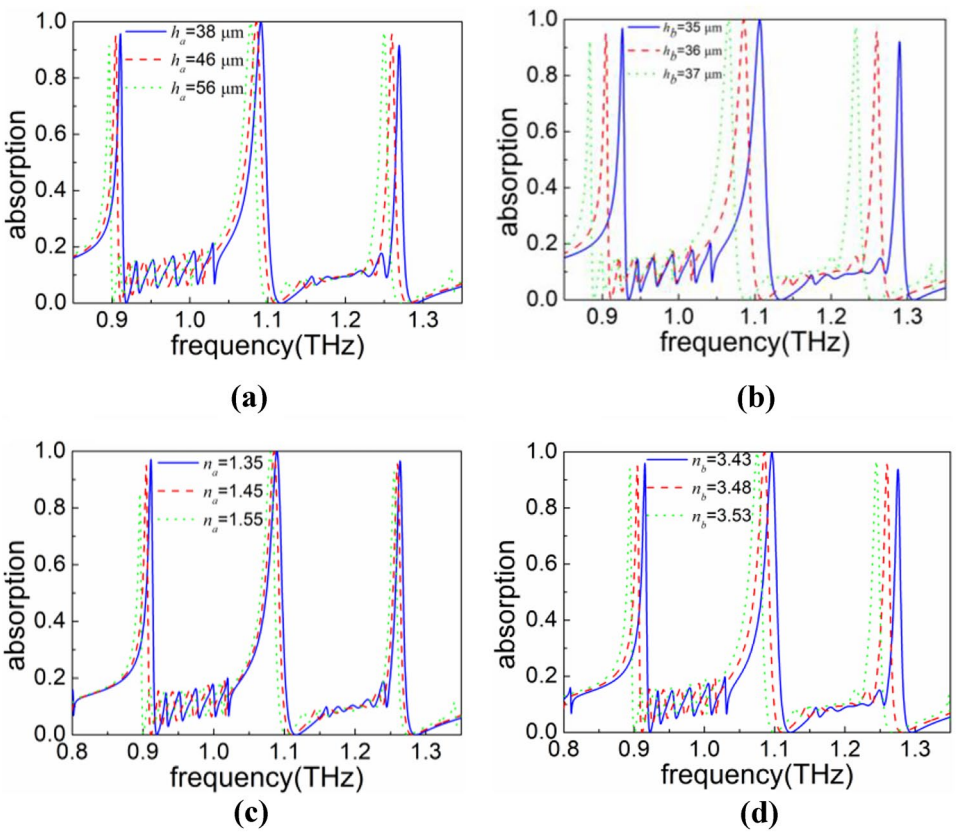

Fig. 5 The simulated absorption spectra for different (**a**) h_a and (**b**) h_b, respectively. The simulated absorption spectra for different (**c**) n_a and (**d**) n_b, respectively

large structure dimension ranges, which will benefit the practical fabrications.

Besides the angle of incidence and the structure dimensions tunability, the designed multichannel absorber is particularly attractive as the absorption properties could be flexibly changed through applying external gate voltages. In Fig. 7a, we plot the simulated absorption spectra versus the varying of the Fermi energy. It is found that the multichannel absorption presents a blueshift with the increase of E_f from 0.70 to 1.0 eV, only with a little decrease or increase for different absorption peaks. Therefore, the multichannel resonant frequencies could be easily changed through a change in the Fermi energy, which will benefit the real application as the absorption properties could be flexibly change without refabricating a new device. In the actual applications, to control the Fermi level of the graphene, two electrodes, one is on the graphene and the another is on the dielectric spacer, can be fabricated by thermal deposition for the gate voltage. Despite a three-channel tunable absorber with $n=6$ is studied here, it could be simply extended to other absorbers with channels of different number by only a change in n. To confirm this characteristic, the calculated absorption spectra for different n are illustrated in Fig. 7b, where the structure dimensions are the same as $n=6$. It can be seen there are two absorption channels for $n=4$ and four absorption channels for $n=9$ in the frequencies range of 0.8–1.35 THz. In addition, the absorptivity remains larger than 90%. This characteristic is especially attractive since the concept could be simply extended without re-designing the structure dimensions.

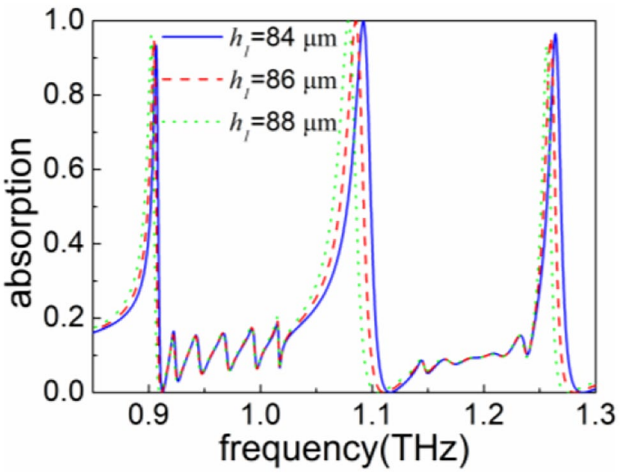

Fig. 6 The simulated absorption spectra versus the varying of h_1

Here, a multichannel tunable THz perfect graphene absorber, in the form of a multilayer planar structure, is proposed and studied. Compared with the conventional metamaterial structure, the multilayer planar structure proposed in this work can be fabricated more easily with lower cost, which is more applicative for practical implementation.

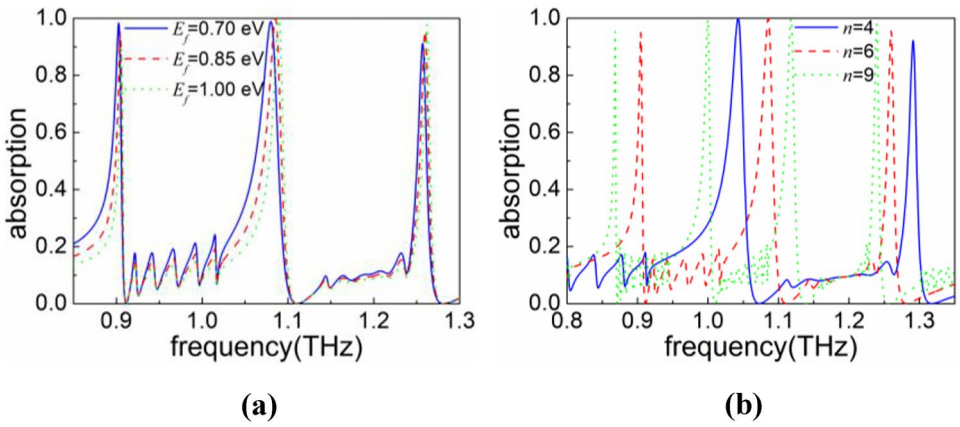

Fig. 7 (**a**) The simulated absorption spectra as a function of Fermi energy; (**b**) the simulated absorption spectra versus the change of *n*

4 Conclusions

In conclusion, tunable multichannel perfect absorption performance in graphene monolayer is studied, which is realized by coating a graphene monolayer on a Fibonacci multilayer separated by a spacer. The results show that graphene TPPs with frequencies locating at different photonic stopbands of the Fibonacci multilayers can be excited, resulting in multichannel near-compete absorption in graphene monolayer. Besides, the absorption properties are insensitive to the polarization state when changing the angle of incidence, which could be employed to tune the multichannel operating frequencies. In addition, the multichannel perfect absorption properties remain excellent within large structure dimension ranges, which should be attractive for practical manufacture. Above all, the multichannel perfect absorption could be flexible tunable through adjusting the Fermi energy and the absorption properties could be easily extended to various absorption channels of different number without redesigning the structure dimensions. It is believed that the results should found significant applications in modulators, thermal emitters [45, 46], photonic detectors [47], and absorber [48–50].

Funding The authors acknowledge the support of the National Natural Science Foundation of China (Grant Nos. 61405217, 52106099), the Zhejiang Provincial Natural Science Foundation (Grant No. LY20F050001), the Anhui Provincial Natural Science Foundation (Grant No. 2108085MF231), the Anhui Polytechnic University Research Startup Foundation (Grant No. 2020YQQ042), the Preresearch Project of National Natural Science Foundation of Anhui Polytechnic University (Grant No. Xjky02202003), and the Natural Science Foundation of Shandong Province (No. ZR2020LLZ004).

Declarations

Conflict of interest The authors declare no competing interests.

References

1. Williams GP (2006) Filling the THz gap-high power sources and applications. Rep Prog Phys 69(2):301–326
2. Tonouchi M (2007) Cutting-edge terahertz technology. Nat Photonics 1(2):97–105
3. Jepsen PU, Cooke DG, Koch M (2011) Terahertz spectroscopy and imaging-modern techniques and applications. Laser Photonics Reviews 5:124–166
4. Wang J, Gou J, Li W (2014) Preparation of room temperature terahertz detector with lithium tantalate crystal and thin film. AIP Adv 4:97–105
5. Diem M, Koschny T, Soukoulis CM (2008) Wide-angle perfect absorber/thermal emitter in the terahertz regime. Phys Rev B Condensed Matter 79:033101
6. Yahiaoui R et al (2018) Multispectral terahertz sensing with highly flexible ultrathin metamaterial absorber. J Appl Phys 118:083103
7. Savo S, Shrekenhamer D, Padilla WJ (2014) Liquid crystal metamaterial absorber spatial light modulator for THz applications. Adv Opt Mater 2:275–279
8. Halterman K, Elson JM (2014) Near-perfect absorption in epsilonnear-zero structures with hyperbolic dispersion. Opt Express 22(6):7337–7348
9. Kakimi R, Fujita M, Nagai M, Ashida M, Nagatsuma T (2014) Capture of a terahertz wave in a photonic-crystal slab. Nat Photonics 8(8):657–663
10. Landy NI, Sajuyigbe S, Mock JJ, Smith DR, Padilla WJ (2008) Perfect metamaterial absorber. Phys Rev Lett 100(20):207402
11. Kenney M, Grant J, Shah YD, Carranza IE, Humphreys M, Cumming DRS (2017) Octave-spanning broadband absorption of terahertz light using metasurface fractal-cross absorbers. ACS Photonics 4(10):2604–2612
12. Bonaccorso F, Sun Z, Hasan T, Ferrari AC (2010) Graphene photonics and optoelectronics. Nat Photonics 4:611–622
13. Zhu Q, Huang Y, Li Y, Zhou M, Xu S, Liu X, Liu C, Yuan B, Guo Z (2021) Aluminum dihydric tripolyphosphate/polypyrrole-functionalized graphene oxide waterborne epoxy composite coatings for impermeability and corrosion protection performance of metals. Adv Compos Hybrid Mater 4:780–792
14. Cao S, Ge W, Yang Y, Huang Q, Wang X (2021) High strength, flexible, and conductive graphene/polypropylene fiber paper fabricated via papermaking process. Adv Compos Hybrid Mater. https://doi.org/10.1007/s42114-021-00374-2
15. Chen L, Zhao Y, Lia M, Lia L, Hou L, Hou H (2021) Reinforced AZ91D magnesium alloy with thixomolding process facilitated

dispersion of graphene nanoplatelets and enhanced interfacial interactions. Mater Sci Eng R Rep A 804:140793
16. Zhao R, Pei J, Du W, Zhao Z, Zhang L, Gao J, Bai P, Tie D (2021) Fabrication of magnesium-coated graphene and its effect on the microstructure of reinforced AZ91 magnesium-matrix composites. Adv Compos Hybrid Mater. https://doi.org/10.1007/s42114-021-00336-8
17. Bao Q, Loh KP (2012) Graphene photonics, plasmonics, and broadband optoelectronic devices. ACS Nano 6:3677–3694
18. Luo X, Yang G, Schubert DW (2021) Electrically conductive polymer composite containing hybrid graphene nanoplatelets and carbon nanotubes: synergistic effect and tunable conductivity anisotropy. Adv Compos Hybrid Mater. https://doi.org/10.1007/s42114-021-00332-y
19. Wu H, Zhong Y, Tang Y, Huang Y, Liu G, Sun W, Xie P, Pan D, Liu C, Guo Z (2021) Precise regulation of weakly negative permittivity in $CaCu_3Ti_4O_{12}$ metacomposites by synergistic effects of carbon nanotubes and grapheme. Adv Compos Hybrid Mater. https://doi.org/10.1007/s42114-021-00378-y
20. Mark KF, Sfeir MY, Wu Y, Lui CH, Misewich JA, Heinz TF (2008) Measurement of the optical conductivity of graphene. Phys Rev Lett 101(19):196405
21. Wu H, Sun H, Han F, Xie P, Zhong Y, Quan B, Zhao Y, Liu C, Fan R, Guo Z (2022) Negative permittivity behavior in flexible carbon nanofibers-polydimethylsiloxane films. Eng Sci 17:113–120
22. Xie P, Zhang Z, Wang Z, Sun K, Fan R (2019) Targeted double negative properties in silver/silica random metamaterials by precise control of microstructures. Research 2019:1021368
23. Koppens FHL, Chang DE, de Abajo FJG (2011) Graphene plasmonics: a platform for strong light-matter interactions. Nano lett 11(8):3370–3377
24. Xia SX, Zhai X, Huang Y, Liu JQ, Wang LL, Wen SC (2017) Multi-band perfect plasmonic absorptions using rectangular graphene gratings. Opt Lett 42(15):3052–3055
25. Alaee R, Farhat M, Rockstuhl C, Lederer F (2012) A perfect absorber made of a graphene micro-ribbon metamaterial. Opt Express 20(27):28017–28024
26. Liu M, Yin X, Ulin-Avila E, Geng B, Zentgraf T, Ju L, Wang F, Zhang X (2011) A graphene-based broadband optical modulator. Nature 474:64–67
27. Wei H, Li A, Kong D, Li Z, Cui D, Li T, Dong B, Guo ZH (2021) Polypyrrole/reduced graphene aerogel film for wearable piezoresisitic sensors with high sensing performances. Adv Compos Hybrid Mater 4:86–95
28. Algadi H, Albargi H, Umar A, Shkir M (2021) Enhanced photoresponsivity of anatase titanium dioxide (TiO2)/nitrogen-doped graphene quantum dots (N-GQDs) heterojunction-based photodetector. Adv Compos Hybrid Mater 4:1354–1366
29. Xia SX, Zhai X, Wang LL, Wen SC (2018) Plasmonically induced transparency in double-layered graphene nanoribbons. Photonics Res 6(7):692–702
30. Zhang Y, Feng Y, Zhu B, Zhao J, Jiang T (2014) Graphene based tunable metamaterial absorber and polarization modulation in terahertz frequency. Opt Express 22(19):22743–22752
31. Deng X-H, Liu J-T, Yuan J, Wang T-B, Liu N-H (2014) Tunable THz absorption in graphene-based heterostructures. Opt Express 22(24):30177–30183
32. He X, Zhong X, Lin F, Shi W (2016) Investigation of graphene assisted tunable terahertz metamaterials absorber. Opt Mater Express 6(2):331–342
33. Zhu L, Liu F, Lin H, Hu J, Yu Z, Wang X, Fan S (2015) Angle-selective perfect absorption with two-dimensional materials. Light Sci Appl 5:e16052
34. Gao RM, Xu ZC, Ding CF, Yao JQ (2016) Intensity-modulating graphene metamaterial for multiband terahertz absorption. Appl Opt 55(8):1929–1933
35. Wang X, Jiang X, You Q, Guo J, Dai X, Xiang Y (2017) Tunable and multichannel terahertz perfect absorber due to Tamm surface plasmons with graphene. Photon Res 5(6):536–542
36. Gong YK, Liu XM, Wang LR, Lu H, Wang G (2011) Multiple responses of TPP-assisted near-perfect absorption in metal/Fibonacci quasiperiodic photonic crystal. Opt Express 19(10):9759–9769
37. Gusynin VP, Sharapov SG, Carbotte JP (2006) Unusual microwave response of Dirac quasiparticles in grapheme. Phys Rev Lett 96(25):256802
38. Gan CH, Chu HS, Li EP (2012) Synthesis of highly confined surface plasmon modes with doped graphene sheets in the midinfrared and terahertz frequencies. Phys Rev B 85(12):125431
39. Moharam MG, Grann EB, Pommet DA, Gaylord TK (1995) Formulation for stable and efficient implementation of the rigorous coupled-wave analysis of binary gratings. J Opt Soc Am A 12:1068–1076
40. Lalanne P, Morris GM (1996) Highly improved convergence of the coupled-wave method for TM polarization. J Opt Soc Am A 13:779–784
41. Kavokin AV, Shelykh IA, Malpuech G (2005) Lossless interface modes at the boundary between two periodic dielectric structures. Phys Rev B 72:233102
42. Kaliteevski M, Iorsh I, Brand S, Abram RA, Chamberlain JM, Kavokin AV, Shelykh IA (2007) Tamm plasmon-polaritons: possible electromagnetic states at the interface of a metal and a dielectric Bragg mirror. Phys Rev B 76:165415
43. Brand S, Kaliteevski MA, Abram RA (2009) Optical Tamm states above the bulk plasma frequency at a Bragg stack/metal interface. Phys Rev B 79:085416
44. Wang X, Hu X, Li Y, Jia W, Xu C, Liu X, Zi J (2002) Enlargement of omnidirectional total-reflection frequency range in one dimensional photonic crystals by using photonic heterostructures. Appl Phys Lett 80(23):4291–4293
45. Xu Z, Luo H, Zhu H, Hong Y, Shen W, Ding J, Kaur S, Ghosh P, Qiu M, Li Q (2021) Nonvolatile optically reconfigurable radiative metasurface with visible tunability for anticounterfeiting. Nano Lett 21:5269–5276
46. Xu Z, Li Q, Du K, Long S, Yang Y, Cao X, Luo H, Zhu H, Ghosh P, Shen W, Qiu M (2020) Spatially resolved dynamically reconfigurable multilevel control of thermal emission. Laser Photon Rev 14:1900162
47. Yu J, Ma B, Ouyang A, Ghosh P, Luo H, Pattanayak A, Kaur S, Qiu M, Belov P, Li Q (2021) Dielectric super-absorbing metasurfaces via PT symmetry breaking. Optica 8(10):1290–1295
48. Xie P, Liu Y, Feng M, Niu M, Liu C, Wu N, Sui K (2021) Rahul Rangrao Patil, Duo Pan, Zhanhu Guo & Runhua Fan Hierarchically porous Co/C nanocomposites for ultralight high-performance microwave absorption. Adv Compos Hybrid Mater 4:173–185
49. Wang W, Deng X, Liu D, Luo F, Cheng H, Cao T, Li Y, Deng Y, Xie W (2021) Broadband radar-absorbing performance of square-hole structure. Adv Compos Hybrid Mater. https://doi.org/10.1007/s42114-021-00376-0
50. Qi G, Liu Y, Chen L, Xie P, Pan D, Shi Z, Quan B, Zhong Y, Liu C, Fan R, Guo Z (2021) Lightweight Fe3C@Fe/C nanocomposites derived from wasted cornstalks with high-efficiency microwave absorption and ultrathin thickness. Adv Compos Hybrid Mater 4:1226–1238